Published in final edited form as:
Cell. 2013 January 31; 152(3): 599–611. doi:10.1016/j.cell.2012.12.028.

Control of Nutrient Stress-Induced Metabolic Reprogramming by PKCζ in Tumorigenesis

Li Ma[1], **Yongzhen Tao**[1], **Angeles Duran**[1], **Victoria Llado**[1], **Anita Galvez**[2], **Jennifer F. Barger**[2], **Elias A. Castilla**[2], **Jing Chen**[2], **Tomoko Yajima**[1], **Aleksey Porollo**[2], **Mario Medvedovic**[2], **Laurence M. Brill**[1], **David R. Plas**[2], **Stefan J. Riedl**[1], **Michael Leitges**[3], **Maria T. Diaz-Meco**[1], **Adam D. Richardson**[1], and **Jorge Moscat**[1,*]

[1]Sanford-Burnham Medical Research Institute, 10901 N. Torrey Pines Road, La Jolla, CA 92037, USA

[2]University of Cincinnati Medical College, Cincinnati, OH 45267, USA

[3]Biotechnology Centre of Oslo, University of Oslo, 0316 Oslo, Norway

SUMMARY

Tumor cells have high-energetic and anabolic needs and are known to adapt their metabolism to be able to survive and keep proliferating under conditions of nutrient stress. We show that PKCζ deficiency promotes the plasticity necessary for cancer cells to reprogram their metabolism to utilize glutamine through the serine biosynthetic pathway in the absence of glucose. PKCζ represses the expression of two key enzymes of the pathway, PHGDH and PSAT1, and phosphorylates PHGDH at key residues to inhibit its enzymatic activity. Interestingly, the loss of PKCζ in mice results in enhanced intestinal tumorigenesis and increased levels of these two metabolic enzymes, whereas patients with low levels of PKCζ have a poor prognosis. Furthermore, PKCζ and caspase-3 activities are correlated with PHGDH levels in human intestinal tumors. Taken together, this demonstrates that PKCζ is a critical metabolic tumor suppressor in mouse and human cancer.

INTRODUCTION

The phenomenon widely known as the Warburg effect describes the ability of tumor cells to rely on aerobic glycolysis to maintain cell growth and proliferation. This provides a rapid way to produce the energy and metabolites required for the high rate of anabolism that drives the dramatically increased proliferation of cancer cells (Vander Heiden et al., 2009). However, although cells undergoing the Warburg effect are empowered to rapidly proliferate when glucose is plentiful, a flexible and adaptive metabolic program would allow them to better respond to changes in nutrient availability and metabolic stress conditions. In addition to glucose, tumor cells can metabolize glutamine, whose transport into the cell is dramatically enhanced during transformation (DeBerardinis and Cheng, 2010; Fuchs and Bode, 2006). Glutamine is a very versatile metabolite because it can not only provide ATP by oxidation through the Krebs cycle but also generate nitrogen for nucleotide synthesis, and

*Correspondence: jmoscat@sanfordburnham.org.

SUPPLEMENTAL INFORMATION

Supplemental Information includes Extended Experimental Procedures, four figures, and one table and can be found with this article online at http://dx.doi.org/10.1016/j.cell.2012.12.028.

ACCESSION NUMBERS

The GEO accession number for the microarray data reported in this paper is GSE42186.

it is a precursor of glutathione, helping to control the side effects of oxidative stress (DeBerardinis and Cheng, 2010).

In theory, therapies aimed at curtailing glucose utilization by "glucose-addicted" cancer cells could be efficacious in treating tumors with relative specificity. However, this approach will invariably trigger nutrient stress, which is often observed in aggressive tumors, even at early stages, and correlates with poor patient survival (Le et al., 2006; Swinson et al., 2003). Signaling molecules that prevent this adaptive response to nutrient stress are predicted to act as tumor suppressors. In this paper, we have addressed this hypothesis in the context of the tumor suppressor role and mechanism of action of PKCζ. This is one of the two members of the atypical PKC family of isoenzymes (aPKCs) whose genetic inactivation in mice leads to enhanced tumorigenesis in a model of Ras-induced lung carcinogenesis (Galvez et al., 2009). Here, we report that PKCζ-deficient cells reprogram their metabolism for the utilization of glutamine instead of glucose through the serine biosynthetic cascade controlled by 3-phosphoglycerate dehydrogenase (PHGDH). This is particularly relevant in light of recent findings suggesting a critical role for this newly identified metabolic cascade in oncogenesis (Locasale et al., 2011; Possemato et al., 2011). Therefore, PKCζ emerges as a critical regulator of tumor metabolism.

RESULTS

Control of Nutrient Stress in Cancer Cells by PKCζ

Our previous studies suggested that the loss of PKCζ in Ras-transformed cells served to confer resistance to stress due to nutrient exhaustion (Galvez et al., 2009). However, the conditions of nutrient scarcity were poorly defined in those studies (Galvez et al., 2009). Here, we sought to investigate the molecular and cellular mechanisms accounting for the tumor suppressor activity of PKCζ as a potential regulator of the cellular response to metabolic stress. We infected SW480 cells with lentivirus expressing PKCζ RNAi (shPKCζ), after which their proliferative properties were compared to those cells with unaltered levels of PKCζ (infected with a control lentivirus; shNT). The elimination of endogenous PKCζ was >90% efficient as determined by immunoblot densitometry (Figure 1A, upper). We next cultured both cell types without subsequent media changes, which led to nutrient exhaustion over time (Figures 1B and 1C). Glucose levels were pronouncedly reduced in the culture medium of the cells incubated under these conditions (Figure 1B). Interestingly, whereas the rate of increase in cell number of the control cells started to decline at day 7 and was completely stalled at day 11, proliferation of PKCζ-deficient cells was not impaired under these conditions (Figure 1D). Cell-cycle analyses demonstrated that, whereas shNT cells underwent massive apoptosis under nutrient-scarce conditions, shPKCζ cells did not (Figure S1A available online). Consistently, cells with reduced levels of PKCζ had lower caspase-3 activity (Figure 1A, middle). No major differences in cell-cycle progression were observed between shNT and shPKCζ cells (Figure S1A). shNT cells depleted glucose from the culture medium more efficiently than shPKCζ cells, even at time points in which shPKCζ cells outnumbered shNT cells (Figures 1B and 1D). shPKCζ cells depleted glutamine from the medium more efficiently than shNT cells (Figure 1C). This indicates that glucose is consumed more actively in shNT than in shPKCζ cells, as confirmed by the data of Figures 1E and 1F showing that shNT cells displayed higher levels of glucose consumption and lactate production than shPKCζ cells. PKCζ-deficient tumor cells were resistant to apoptosis induced by glucose deprivation (Figures S1B and 1G). These observations were also confirmed in other human cancer cells and with three different shRNAs of PKCζ (Figures S1C and S1D). We have been able to maintain shPKCζ but not shNT cells in culture in the absence of glucose for prolonged times, with glucose-free medium change every 2 days (Figure S1E). Reconstitution of shPKCζ cells with wild-type (WT) but not with kinase-dead PKCζ completely abolished the enhanced proliferation of

shPKCζ cells (Figure 1H), demonstrating that PKCζ-deficient cells are able to activate an emergency mechanism in response to nutrient stress caused by the lack of glucose. Consistently, ATP levels are dramatically reduced in shNT cells in the absence of glucose but are maintained at normal levels in viable shPKCζ (Figure S1F). SW620, a more aggressive variant of SW480, displayed little or no PKCζ (Figure S1G). Interestingly, similarly to SW480 shPKCζ cells, SW620 cells were able to survive and proliferate under nutrient stress conditions (Figure S1H). Consistently, WT but not kinase-dead PKCζ was able to repress the ability of SW620 cells to resist nutrient stress (Figure 1I).

Role of PKCζ in Stress Signaling in Response to Glucose Deprivation

We performed experiments to establish the mechanisms whereby PKCζ deficiency allows cell proliferation under conditions of nutrient deprivation. Nutrient exhaustion (Figure 2A) or incubation of cells under glucose-free conditions (Figure 2B) both led to activation of PKCζ and its nuclear translocation, whereas the other aPKC, PKCλ/ι, was not affected (Figures 2C, S2A, and S2B). Ser-311 phosphorylation of a bona fide substrate of PKCζ (RelA; Duran et al., 2003) in immunoprecipitates from the same extracts of Figure 2A independently confirms that PKCζ is activated during nutrient exhaustion (Figure 2A, lowest two panels). Consistent with the requirement for glucose to maintain the energetic demands of cancer cells, AMPK was activated in shNT cells incubated in glucose-free culture medium (Figures 2D and S2B). Intriguingly, reduction in PKCζ levels led to lower amounts of phospho-AMPK under these conditions (Figure 2D). Phospho-ACC and phospho-ULK1 levels were in keeping with elevated AMPK activity (Figure 2D). Autophagy was induced in shNT cells in response to glucose deprivation, but this induction was significantly inhibited in PKCζ-deficient cells (Figure 2D). Increased LC3-II levels can be a consequence of enhanced autophagy or decreased autophagic flux. To determine which of these two effects could account for the results in Figure 2D, we incubated shNT and shPKCζ cells in the absence of glucose, with or without a combination of two protease inhibitors (E64 and pepstatin) that interrupt autophagic flux as determined by the accumulation of LC3-II (Figure 2E). These data demonstrate that PKCζ deficiency results in decreased AMPK activation and autophagy when cancer cells are incubated in glucose-free conditions. mTOR activity, which is normally shut down under conditions of energy depletion, is likewise inhibited in glucose-free medium in shNT but not in shPKCζ cells (Figure 2D). These results demonstrate a direct or indirect role for PKCζ in the biochemical response to nutrient stress activated by the lack of glucose in cells that require this nutrient for survival and growth.

AMPK and autophagy are two survival mechanisms set in motion by cells under low energetic environments (Hardie, 2007; Kroemer et al., 2010). The activation of fatty acid oxidation and autophagy, two processes under the control of AMPK, are mechanisms that result in enhanced cell survival. Consistent with the AMPK/ACC results (Figure 2D), PKCζ deficiency impaired the enhanced fatty acid oxidation triggered by glucose deprivation (Figure 2F). Interestingly, in the absence of glucose, shNT cells exhibited increased JNK activity and the expression of its downstream target c-Jun (Figures 2G and S2B). In contrast, the activation of this pathway was completely blunted in shPKCζ cells under identical culture conditions (Figure 2G). Similarly, the activation of JNK, which was dramatically activated in WM35 melanoma cells cultured in the absence of glucose, was completely inhibited in PKCζ-deficient WM35 cells (Figure S2C). One interpretation of these results is that PKCζ deficiency prevents nutrient stress in cancer cells, which is translated into a failure to activate the biochemical emergency signals that are normally set in motion when cells sense a potential energetic or metabolic catastrophe. Therefore, PKCζ-deficient cells do not shut down their anabolic activities, as manifested by a lack of effect on mTORC1

activity, when incubated in glucose-free conditions (Figure 2D), as well as by the ability of PKCζ-deficient cells to proliferate under nutrient stress (Figures 1D and S1E).

Role of Stress Signaling in Cell Proliferation in the Absence of Glucose

One possibility is that all the biochemical stress-induced signaling is the consequence, rather than the cause, of an enhanced energetic and metabolic state of PKCζ-deficient cells growing under glucose-deprived conditions. Therefore, inhibition of these parameters in shNT cells should have no impact on the failure to survive and proliferate in the absence of glucose. To address the role of autophagy, we generated ATG5-deficient cells (shATG5) and asked whether the inhibition of autophagy in shNT cells was sufficient to promote cell growth in the absence of glucose. ATG5 levels were reduced in SW480 cells infected with shRNA for ATG5, and that autophagy was impaired as detected by the accumulation of p62 (Figure S2D). Impaired autophagy in shNT cells did not result in enhanced cell survival and proliferation under glucose-free conditions (Figure S2E). Similarly, activation of AMPK with AICAR in shPKCζ cells, or inhibition of AMPK with compound C in shNT cells, did not affect the ability of shPKCζ cells to grow nor did it change the ability of shNT cells to be rescued from a lack of proliferation in glucose-free medium (Figure S2F). We next generated SW480 cells with normal (shNT) or depleted levels of AMPK (shAMPK) in a shNT or shPKCζ background and determined their ability to proliferate in glucose-free medium. AMPK was knocked down in both cell lines (Figure S2G). AMPK deficiency does not affect the proliferative properties of shNT or shPKCζ cells in glucose-free conditions (Figure S2H). Also, SP600125-induced inhibition of JNK did not allow shNT cells to grow in glucose-free medium (Figure S2I). JNK knockdown had no effect on the response of either cell line to glucose deprivation (Figures S2J and S2K). These results indicate that the lack of stress signaling in glucose-deprived PKCζ-deficient cells cannot explain their higher proliferative response. One possibility is that PKCζ-deficient cells are able to reprogram their metabolism for the efficient utilization of fuels other than glucose, allowing them to survive and proliferate in the absence of that nutrient.

Cancer Metabolic Control by PKCζ

Genome-wide transcriptome analysis demonstrated that PKCζ-deficient cells displayed gene alterations in pathways consistent with the use of glutamine as a glucose alternative ($p = 1.1 \times 10^{-39}$; $FDR = 2.79 \times 10^{-36}$; Table S1). In fact, shPKCζ cells consumed glutamine more rapidly than did the shNT cells (Figure 3A), suggesting that the ability to utilize glutamine as the primary carbon source underlies the survival advantage of shPKCζ cells when glucose is limited. We next grew shNT and shPKCζ cells in media that contained glutamine as the sole metabolic substrate. In separate experiments, the glutamine present in the media was composed of either ^{15}N at the α-nitrogen, or ^{13}C at all carbon positions. ^{15}N incorporation into both serine and glycine was significantly increased in the shPKCζ cells, indicating that the PHGDH/PSAT pathway was more active in this cell line (Figures 3B and 3C). No difference was found in aspartate or alanine biosynthesis under these conditions (Figure S3A). When cells were labeled with ^{13}C-glutamine under the same conditions, the entire serine-glycine biosynthetic pathway was specifically increased in the shPKCζ cells as evidenced by increased labeling of 3-phosphoglycerate (3PG), serine, and glycine (Figure 3D, left, white and black bars), whereas other glutamine-utilizing pathways remained unchanged (Figures S3B–S3D). This suggests that the serine biosynthetic pathway is a primary mechanism for glutamine utilization in the shPKCζ cells. Gene expression analysis of enzymes in this pathway demonstrated that PKCζ deficiency resulted in increased expression of PSAT1 and PHGDH at the mRNA and protein level (Figures 3E and 3F). The reconstitution of shPKCζ cells with WT but not with kinase-dead PKCζ significantly reduced the increase in PHGDH in shPKCζ cells (Figure 3G). PHGDH catalyzes the conversation of 3PG to 3-phosphohydroxypyruvate (3PHP) (Figure 3C). PSAT then

converts 3PHP to phosphoserine in a biochemical reaction that transfers the α-nitrogen of glutamate to 3PHP while producing α-ketoglutarate (Figure 3C). This can be interpreted to mean that at least one of the important tumor-suppressing functions of PKCζ is to prevent nutrient stress cells from redirecting their metabolism to a more efficient utilization of glutamine. Phosphoserine phosphatase (PSPH), the enzyme that catalyzes the final step of serine biosynthesis, was not significantly increased (Figure S3E), suggesting that it is indeed the α-ketoglutarate-producing portion of this pathway that is most critical for cell survival (Figure 3C). The expression of other aminotransferases was unchanged (Figure S3E).

To test the relevance of this metabolic pathway, we simultaneously knocked down PKCζ and PHGDH. PHGDH reduction impaired serine and glycine production from ^{13}C-glutamine even in shPKCζ cells, demonstrating the effective inactivation of this metabolic cascade (Figure 3D). Furthermore, the knockdown of PHGDH levels not only impairs serine and glycine production but also the generation of 3PG (Figure 3D). This indicates that the regulation of PHGDH by PKCζ is essential to activate glutamine metabolism to produce 3PG and to activate the serine/glycine pathway. Importantly, the loss of either PHGDH or PSAT1 completely abolished the proliferation of PKCζ-deficient cells in the absence of glucose (Figures 3H and 3I). Furthermore, the simultaneous knockdown of PKCζ and either PSAT1 or PHGDH restores the activation of AMPK and JNK in the PKCζ-deficient cells to levels comparable to those of shNT cells when all are incubated in the absence of glucose (Figure 3J). This supports the idea that PKCζ is not a direct regulator of the biochemical stress signals but rather regulates the metabolic state of the cell, which in turn modulates the stress signal transduction pathways.

Regulation of PHGDH by PKCζ Phosphorylation

Based on these observations, we would predict that the overexpression of PHGDH in SW480 cells with normal levels of PKCζ should be sufficient to confer these cells resistance to nutrient stress. However, the simple overexpression of PHGDH is not sufficient to confer SW480 cells the ability to survive and proliferate under nutrient-scarce conditions (Figure 4A). Metabolic analysis demonstrates the lack of differences between SW480 cells that overexpress and those that do not overexpress PHGDH (data not shown). One potential explanation to these observations is that PKCζ, in addition to lowering PHGDH levels, would also directly repress PHGDH activity by direct phosphorylation. Interestingly, our data demonstrate that PHGDH is a bona fide direct substrate of PKCζ (Figure 4B). To determine the phosphorylated residues of PHGDH, titanium dioxide (TiO2)-based phosphopeptide enrichment was performed on tryptic digests of in vitro-phosphorylation reactions, followed by HPLC-tandem mass spectrometry (MS/MS) analysis. MS/MS spectra showed that PKCζ phosphorylates PHGDH at residues Ser55, Thr57, and Thr78 (Figure 4C). These three residues were not phosphorylated in PKCζ- or PHGDH-only controls and are highly conserved among species, and according to the structure of PHGDH (Protein Data Bank ID code 2g76), might play critical roles in its activity (Figures 4D and 4E). Thr78 lies adjacent to both the substrate and cofactor binding sites, and mutation of this residue would predictably directly decrease binding efficiencies in both sites (Figure 4E). Thr57 does not directly contact either ligand but plays an important role stabilizing the loop harboring Ser55 as well as Arg54, which synergizes with Arg135 directly adjacent to the expected position of the substrate 3-phospho-D-glycerate. A previous study has identified an Arg135 missense mutation in PHGDH deficiency (Tabatabaie et al., 2009). Therefore, mutations of Thr57 will likely cause a similar effect by destabilizing the loop where Arg54 resides and, thus, abrogating substrate binding. To test these predictions, we independently mutated Ser55, Thr57, and Thr78 and determined the impact that these mutations have on the enzymatic activity in vitro. T→A and T→E mutations of Thr57 severely abrogated PHGDH activity (Figure 4F). Although identical mutations of Thr78 have a lower impact on

PHGDH's V_{max}, however, the T→E mutation severely affected the K_M (Figure 4G). S→E mutation of Ser55 reproducibly inhibited PHGDH activity to a greater extent than S→A mutation (Figure 4H). A construct harboring a triple 55/57/78 E or A mutant completely abrogated PHGDH activity (Figure 4I). Also, the in vitro phosphorylation of PHGDH by PKCζ results in a significant inhibition of PHGDH's enzymatic activity (Figure 4J). Collectively, these results demonstrate that PHGDH's Ser55, Thr57, and Thr78 are functionally relevant targets of PKCζ. We next treated shNT and shPKCζ cells under normal or glucose-deprivation conditions, after which PHGDH was immunoprecipitated and analyzed by immunoblotting with an anti-phospho-Thr antibody. Results of Figure 4K demonstrate that PHGDH is Thr phosphorylated at 48 hr under glucose-deprived conditions in a PKCζ-dependent manner, consistent with the kinetic of PHGDH induction levels shown in Figure 3F. We did not observe increased serine phosphorylation of PHGDH upon glucose deprivation under similar conditions (data not shown). To further determine whether the PKCζ-targeted-identified residues are actually phosphorylated in vivo, we generated SW480 cells expressing flag-tagged PHGDH in either WT or a triple S55/T57/T78 mutant. Interestingly, although glucose deprivation resulted in a robust Thr phosphorylation of WT PHGDH at 48 hr, as in the previous experiment (compare Figures 4K and 4L), this phosphorylation was undetectable in the PHGDH triple mutant (Figure 4L). This phosphorylation event was not detected at earlier time points, including 24 hr (Figure S4). These results demonstrate that PGHDH is phosphorylated by PKCζ at the identified residues in vivo under conditions of nutrient stress. To confirm the functional relevance of these phosphorylations, MDA-MB-231 cells, which have low PKCζ levels and undetectable levels of PHGDH, were transfected with WT or triple-mutant PHGDH and were incubated under conditions of serine deprivation, after which their ability to survive and proliferate was determined by trypan blue exclusion assay. Interestingly, WT PHGDH, but not its triple mutant, conferred MDA-MB-231 cells the ability to proliferate under these conditions (Figure 4M). Collectively, these results indicate that PHGDH Thr57 and Thr78 are most likely the inducible phosphorylation substrates of PKCζ in cells under nutrient stress and that they play critical roles in PHGDH activity and functions accounting for the involvement of PKCζ as a metabolic tumor suppressor.

Tumor-Suppressive Role of PKCζ in Intestinal Cancer

We next sought to determine whether the loss of PKCζ in intestinal tumors also results in increased levels of PHGDH, PSAT1, or both, correlating with enhanced carcinogenesis and reduced apoptosis. To generate the tumor samples needed to address this question, we crossed PKCζ knockout (KO) mice with $APC^{Min/+}$ mice (widely accepted model of intestinal tumorigenesis). Kaplan-Meier survival plots for $APC^{Min/+}PKC\zeta^{-/-}$ versus $APC^{Min/+}PKC\zeta^{+/+}$ mice demonstrated that the lack of PKCζ promoted intestinal cancer. $APC^{Min/+}PKC\zeta^{-/-}$ mice exhibited a median survival of 26 weeks, whereas 100% of $APC^{Min/+}PKC\zeta^{+/+}$ mice were alive at 30 weeks, which was the extent of the duration of the study (Figure 5A, open symbols). Another set of mutant mice was fed a Western diet (WD) to accelerate the appearance of tumors (Baltgalvis et al., 2009). Under these conditions, 100% of the $APC^{Min/+}PKC\zeta^{-/-}$ KO mice had died at 26 weeks of treatment, with a median survival of 22 weeks, whereas 80% of the $APC^{Min/+}PKC\zeta^{+/+}$ mice were still alive at that time (Figure 5A, filled symbols). Therefore, $APC^{Min/+}PKC\zeta^{-/-}$ mice died significantly earlier than $APC^{Min/+}PKC\zeta^{+/+}$ littermate controls, independent of the diet. There were also significant differences in weight gain between $APC^{Min/+}PKC\zeta^{+/+}$ and $APC^{Min/+}PKC\zeta^{-/-}$ mice after 4 weeks on the WD (Figure 5B). The weight loss of the $APC^{Min/+}PKC\zeta^{-/-}$ group after 8 weeks on the WD, along with the appearance of other detrimental conditions such as anemia, rectal prolapse, and limited survival, dictated the completion of the study when the mice were 16–18 weeks old. PKCζ deficiency induced a higher total number of polyps (Figures 5C and 5D), and these were larger (tumor area) than those in $PKC\zeta^{+/+}$ mice (Figure

5E). $APC^{Min/+}PKC\zeta^{-/-}$ tumors were also more aggressive than those in $APC^{Min/+}PKC\zeta^{+/+}$ mice, with adenomas with significant nuclear atypia (including vesicular nuclei, prominent nuclei, and a loss of nuclear polarity) and marked architectural distortion frequently including a cribriform pattern of growth (adenomas with high-grade dysplasia) (Figure 5F). Areas with more significant cribri-forming and an expanding-type infiltration into the lamina propria by back-to-back glands (intramucosal adenocarcinoma) were also identified in the PKCζ-deficient $APC^{Min/+}$ tumors (Figure 5G). The majority of these lesions displayed strong staining for β-catenin (Figures 5H and 5I). In contrast, $APC^{Min/+}PKC\zeta^{+/+}$ mice showed either single dysplastic crypts or several adjacent dysplastic glands with moderate nuclear pleomorphism but preservation of nuclear polarity and absence of a complex architecture (adenomas with low-grade dysplasia) (Figure 5F). Collectively, these results indicate that the genetic inactivation of PKCζ leads to increased intestinal tumorigenesis by APC inactivation, which is consistent with a role for PKCζ as a tumor suppressor. Analysis of Affymetrix mouse genome arrays (Gene Expression Omnibus [GEO] data set DS389) (Paoni et al., 2003) demonstrated significant PKCζ downregulation in adenomas and adenocarcinomas from $APC^{Min/+}$ mice as compared with normal tissue from the same mouse line and when $APC^{Min/+}$ samples were compared with WT control mice (Figure 5J).

PKCζ Loss Reduced Apoptosis in the Cancerous Intestine of $APC^{Min/+}$ Mice and Humans

No changes in Ki67 staining were observed in $APC^{Min/+}PKC\zeta^{-/-}$ tumors as compared with $APC^{Min/+}PKC\zeta^{+/+}$ controls (Figures 6A and 6B). In contrast, PKCζ deficiency led to a reduction in the number of activated caspase-3-positive cells in $APC^{Min/+}$ tumors (Figures 6C and 6D). To test the physiological relevance of the increased expression of PHGDH and PSAT1 induced by PKCζ deficiency in cultured SW480 cells, we analyzed these two mRNAs in tumor samples from $APC^{Min/+}$ mice with or without PKCζ deficiency. Importantly, PHGDH and PSAT1 were significantly increased in PKCζ-deficient tumors as compared with WT (Figure 6E). To further link the metabolic effects of PKCζ deficiency in cell culture experiments to the in vivo phenotype of PKCζ-deficient $APC^{Min/+}$ mice, tumor explants from these mice and their corresponding $APC^{Min/+}$ WT littermates were incubated with ^{15}N-labeled glutamine for 24 hr, after which the labeling into serine and glycine was determined as above. Interestingly, ^{15}N-glutamine-derived labeling into serine and glycine was significantly increased in the PKCζ-deficient tumors as compared with their counterpart WT controls (Figure 6F).

We next subcutaneously implanted shNT or shPKCζ cells in nude mice. Interestingly, the growth rate of PKCζ-deficient xenografts (shPKCζ) was higher in comparison with those derived from control cells (shNT). PKCζ-deficient xenograft volume was significantly increased by day 39 and continued to increase until day 46 (Figure 6G). Cells with double PHGDH and PKCζ knockdown were unable to form xenograft tumors, consistent with the notion that PHGDH is critical for tumor progression (data not shown). These results demonstrate that PKCζ is a tumor suppressor likely by controlling the ability of cancer cells to respond to nutrient stress by acting upstream of PHGDH. In keeping with this, gene expression analysis of publicly available microarray data demonstrated that PKCζ is downregulated in human colorectal cancers as compared with normal colon tissue (GEO data set GSE5206) (Kaiser et al., 2007) and underexpressed in cancers progressing to metastasis (Figure 7A) (GEO data set GSE6988) (Ki et al., 2007). In addition, we analyzed a human colorectal cancer data set (GEO data set GSE14333) (Jorissen et al., 2009) that included expression data from 290 primary colorectal cancers of different Dukes stages. When patients with stages B and C were stratified in low and high PKCζ groups, it became clear that those with low PKCζ levels showed a statistically significant decrease in disease-free survival (Figure 7B). Analysis of PKCζ expression in a tissue microarray (TMA) consisting of 66 samples of colon cancer tissues yielded similar results. Importantly, 42%

(28 of 66) of the colon adenocarcinomas analyzed were negative for PKCζ expression in the nucleus (Figures 7C and 7D). Samples with decreased nuclear PKCζ staining also showed diminished staining for activated caspase-3, as compared with tissues that stained positively for PKCζ (Figures 7C and 7D). Therefore, human tumor tissues show a positive correlation between PKCζ levels and caspase-3 activation. This is consistent with data from the $APC^{Min/+}$ mouse model, which showed lower activated caspase-3 activity in PKCζ-deficient tumors (Figures 6C and 6D), and from SW480 cells with reduced levels of PKCζ, which had lower caspase-3 activity than control cells (Figures 1A and 1G). When the same TMA was analyzed for PHGDH expression, we found a significant negative correlation between nuclear PKCζ and PHGDH levels (Figures 7C and 7E), demonstrating that the link between PKCζ and this critical metabolic enzyme is also apparent in human patients with cancer. Consistent with PKCζ playing a negative role in this serine-glycine pathway, Figure 7F demonstrates a statistically significant inverse correlation between the expression levels of PKCζ and PSAT1 in human patients with colorectal cancer (GEO data set GSE20916) (Skrzypczak et al., 2010). Collectively, these results demonstrate that PKCζ is a tumor suppressor in intestinal cancer, in both mice and humans.

DISCUSSION

Understanding the differences between normal and tumor cells with regard to metabolic homeostasis could provide an opportunity for selective therapies in cancer. Considerable attention has been paid to the metabolism of glucose in the tumor cell, which has some characteristic features that could be exploited therapeutically. However, the metabolism of cancer cells is much more complex, and recent studies have implicated the direct action of oncogenes and tumor suppressors as potential modulators of this function. In this regard, a key characteristic of the tumor cell is plasticity manifested by a capacity to adapt to the harsh conditions in which the tumor must expand, thus continuing to satisfy the high demand for energy and anabolic building blocks necessary for characteristic uncontrolled growth and survival. This is of particular interest because some clinical data show that tumors may be able to survive therapy by reprogramming their metabolic needs (Ma et al., 2009). This, and the results shown here, has important implications for the metabolic cancer therapeutics aimed at curtailing the supply or utilization of glucose. Such treatments could trigger reprogramming of the metabolic homeostasis of cancer cells, allowing for the efficient utilization of alternative nutrients and metabolic pathways for growth, thus increasing tumor aggressiveness. In this regard, our data demon strate that PKCζ is a determinant of metabolic plasticity and suggest that attacking the Warburg effect would actually be effective in cancer therapy as long as PKCζ is activated.

Our findings demonstrate that PKCζ deficiency allows glucose-addicted human cancer cells to reprogram their metabolism in response to glucose deprivation by increasing the utilization of glutamine through a pathway that involves the generation of 3PG, which is channeled through the serine synthetic cascade due to the regulation of PHGDH and PSAT1, two critical components of this metabolic pathway. Recent studies support the relevance of the serine biosynthetic pathway in cancer. Locasale et al. found that certain cancer cells divert a large amount of glycolytic carbon to the serine biosynthetic pathway, as indicated by amplification of the metabolic enzyme PHGDH (Locasale et al., 2011). They showed that cell proliferation was severely attenuated by downregulation of PHGDH in cells with an amplified PHGDH gene (Locasale et al., 2011). Conversely, overexpression of PHGDH in normal mammary epithelial cells resulted in phenotypic alterations, which suggested that, although not transformed, these cells would be prone to becoming malignant (Locasale et al., 2011). The channeling of glycolytic products to this pathway might have a number of metabolic advantages that could explain why the overexpression of PHGDH triggered certain protumorigenic functions and its depletion impaired tumor cell proliferation in

cancer cells with high PHGDH copy number. Interestingly, another recent study by Possemato et al. (2011) also established the 3PG→serine pathway as relevant in cancer but showed that the production of serine from glycolytic intermediates through this mechanism was not likely to account for the metabolic advantage of PHGDH-overexpressing cells. They proposed that the utilization of glutamine to produce a-ketoglutarate coupled to the conversion of phospho-hydroxypyruvate to phosphoserine by PSAT1 was the relevant step for tumorigenesis (Possemato et al., 2011).

In summary, our data show that in addition to glucose utilization, the reprogramming of cellular metabolism to produce serine from glutamine underscores the importance of serine biosynthesis for tumor cell survival and establishes PKCζ as a critical player in this important metabolic pathway for cancer.

EXPERIMENTAL PROCEDURES

Mice

The PKC$\zeta^{-/-}$ and APC$^{Min/+}$ mice were described previously (Leitges et al., 2001; Moser et al., 1990). All mice were born and maintained under pathogen-free conditions. Animal handling and experimental procedures conformed to institutional guidelines (Institutional Animal Care and Use Committee). All genotyping was done by PCR. The WD (D12079B; OpenSource Diets) was available ad libitum. Mice were sacrificed, and sections of the small intestines, distal to the stomach and proximal to the cecum, were carefully dissected. Mesentery tissue was removed, and the intestine sections were flushed with PBS, fixed in 10% buffered formalin for 24 hr and transferred to 70% ethanol for processing and sectioning. Histological examination was performed on hematoxylin and eosin (H&E)-stained sections.

Cell Culture

SW480, SW620, MW35, and MDA-MB-231 cells were from ATCC. Cells were cultured in Dulbecco's modified Eagle's medium (DMEM) supplemented with 10% fetal bovine serum (FBS), 1% glutamine, and 1% penicillin-streptomycin, in an atmosphere of 95% air and 5% CO_2. Lentiviruses for the different target genes were made as follows: shRNA-encoding plasmids were cotransfected with psPAX2 and pMD2.G packaging plasmids into actively growing HEK293T cells by using FuGENE 6 transfection reagent. Virus-containing supernatants were collected 48 hr after transfection and filtered to remove cells, and target cells were infected in the presence of 8 μg/ml polybrene. Cells were selected with puromycin after infection. Retroviruses for the different target genes were made as follows: pWZL-encoding and pBabe-encoding plasmids were transfected into actively growing Phoenix cells by using FuGENE 6 transfection reagent. Virus-containing supernatants were collected and treated as above, and target cells were infected in the presence of 8 μg/ml polybrene. Cells were selected with hygromycin or puromycin.

Viability Assay and Cell-Cycle Analysis

Cells were seeded onto 6-well plates in 10% FBS-DMEM, washed with PBS twice after attachment, and changed to the indicated medium. Cell viability was determined by trypan blue exclusion assay at the indicated time. For cell-cycle analysis, cells were seeded as above and fixed in ethanol and analyzed by propidium iodide (PI) staining (50 μg/ml in PBS) and flow cytometry (FACScan; Becton Dickinson).

Statistical Analysis

Significant differences between groups were determined using the Student's t test. The differences between intensity of immunostaining in human TMAs were evaluated using

Fisher's exact test as implemented in the SAS statistical software. The significance level for statistical testing was set at $p < 0.05$.

Supplementary Material

Refer to Web version on PubMed Central for supplementary material.

Acknowledgments

NIH Grants R01CA132847 (to J.M.), R01AI072581 (to J.M.), R01DK088107 (to J.M.), R01CA134530 (to M.T.D.-M.), R21CA147978 (to A.D.R.), and CCSG Pilot Project Grant (to J.M. and A.D.R.) funded this work. We thank Maryellen Daston for editing this manuscript, Diantha LaVine for the artwork, and the technical assistance of Tom Hudson, Jessica Leung, and Nahid Hamidy.

REFERENCES

Baltgalvis KA, Berger FG, Peña MM, Davis JM, Carson JA. The interaction of a high-fat diet and regular moderate intensity exercise on intestinal polyp development in Apc Min/+ mice. Cancer Prev. Res. (Phila.). 2009; 2:641–649. [PubMed: 19549797]

DeBerardinis RJ, Cheng T. Q's next: the diverse functions of glutamine in metabolism, cell biology and cancer. Oncogene. 2010; 29:313–324. [PubMed: 19881548]

Duran A, Diaz-Meco MT, Moscat J. Essential role of RelA Ser311 phosphorylation by zetaPKC in NF-kappaB transcriptional activation. EMBO J. 2003; 22:3910–3918. [PubMed: 12881425]

Fuchs BC, Bode BP. Stressing out over survival: glutamine as an apoptotic modulator. J. Surg. Res. 2006; 131:26–40. [PubMed: 16154153]

Galvez AS, Duran A, Linares JF, Pathrose P, Castilla EA, Abu-Baker S, Leitges M, Diaz-Meco MT, Moscat J. Protein kinase Czeta represses the interleukin-6 promoter and impairs tumorigenesis in vivo. Mol. Cell. Biol. 2009; 29:104–115. [PubMed: 18955501]

Hardie DG. AMP-activated/SNF1 protein kinases: conserved guardians of cellular energy. Nat. Rev. Mol. Cell Biol. 2007; 8:774–785. [PubMed: 17712357]

Jorissen RN, Gibbs P, Christie M, Prakash S, Lipton L, Desai J, Kerr D, Aaltonen LA, Arango D, Kruhøffer M, et al. Metastasis-Associated Gene Expression Changes Predict Poor Outcomes in Patients with Dukes Stage B and C Colorectal Cancer. Clin. Cancer Res. 2009; 15:7642–7651. [PubMed: 19996206]

Kaiser S, Park YK, Franklin JL, Halberg RB, Yu M, Jessen WJ, Freudenberg J, Chen X, Haigis K, Jegga AG, et al. Transcriptional recapitulation and subversion of embryonic colon development by mouse colon tumor models and human colon cancer. Genome Biol. 2007; 8:R131. [PubMed: 17615082]

Ki DH, Jeung HC, Park CH, Kang SH, Lee GY, Lee WS, Kim NK, Chung HC, Rha SY. Whole genome analysis for liver metastasis gene signatures in colorectal cancer. Int. J. Cancer. 2007; 121:2005–2012. [PubMed: 17640062]

Kroemer G, Mariño G, Levine B. Autophagy and the integrated stress response. Mol. Cell. 2010; 40:280–293. [PubMed: 20965422]

Le QT, Chen E, Salim A, Cao H, Kong CS, Whyte R, Donington J, Cannon W, Wakelee H, Tibshirani R, et al. An evaluation of tumor oxygenation and gene expression in patients with early stage non-small cell lung cancers. Clin. Cancer Res. 2006; 12:1507–1514. [PubMed: 16533775]

Leitges M, Sanz L, Martin P, Duran A, Braun U, García JF, Camacho F, Diaz-Meco MT, Rennert PD, Moscat J. Targeted disruption of the zetaPKC gene results in the impairment of the NF-kappaB pathway. Mol. Cell. 2001; 8:771–780. [PubMed: 11684013]

Locasale JW, Grassian AR, Melman T, Lyssiotis CA, Mattaini KR, Bass AJ, Heffron G, Metallo CM, Muranen T, Sharfi H, et al. Phosphoglycerate dehydrogenase diverts glycolytic flux and contributes to oncogenesis. Nat. Genet. 2011; 43:869–874. [PubMed: 21804546]

Ma WW, Jacene H, Song D, Vilardell F, Messersmith WA, Laheru D, Wahl R, Endres C, Jimeno A, Pomper MG, Hidalgo M. [18F]fluorodeoxyglucose positron emission tomography correlates with

Akt pathway activity but is not predictive of clinical outcome during mTOR inhibitor therapy. J. Clin. Oncol. 2009; 27:2697–2704. [PubMed: 19380450]

Moser AR, Pitot HC, Dove WF. A dominant mutation that predisposes to multiple intestinal neoplasia in the mouse. Science. 1990; 247:322–324. [PubMed: 2296722]

Paoni NF, Feldman MW, Gutierrez LS, Ploplis VA, Castellino FJ. Transcriptional profiling of the transition from normal intestinal epithelia to adenomas and carcinomas in the APCMin/+ mouse. Physiol. Genomics. 2003; 15:228–235. [PubMed: 13130079]

Possemato R, Marks KM, Shaul YD, Pacold ME, Kim D, Birsoy K, Sethumadhavan S, Woo HK, Jang HG, Jha AK, et al. Functional genomics reveal that the serine synthesis pathway is essential in breast cancer. Nature. 2011; 476:346–350. [PubMed: 21760589]

Skrzypczak M, Goryca K, Rubel T, Paziewska A, Mikula M, Jarosz D, Pachlewski J, Oledzki J, Ostrowski J. Modeling oncogenic signaling in colon tumors by multidirectional analyses of microarray data directed for maximization of analytical reliability. PLoS One. 2010; 5:e13091. [PubMed: 20957034]

Swinson DE, Jones JL, Richardson D, Wykoff C, Turley H, Pastorek J, Taub N, Harris AL, O'Byrne KJ. Carbonic anhydrase IX expression, a novel surrogate marker of tumor hypoxia, is associated with a poor prognosis in non-small-cell lung cancer. J. Clin. Oncol. 2003; 21:473–482. [PubMed: 12560438]

Tabatabaie L, de Koning TJ, Geboers AJ, van den Berg IE, Berger R, Klomp LW. Novel mutations in 3-phosphoglycerate dehydrogenase (PHGDH) are distributed throughout the protein and result in altered enzyme kinetics. Hum. Mutat. 2009; 30:749–756. [PubMed: 19235232]

Vander Heiden MG, Cantley LC, Thompson CB. Understanding the Warburg effect: the metabolic requirements of cell proliferation. Science. 2009; 324:1029–1033. [PubMed: 19460998]

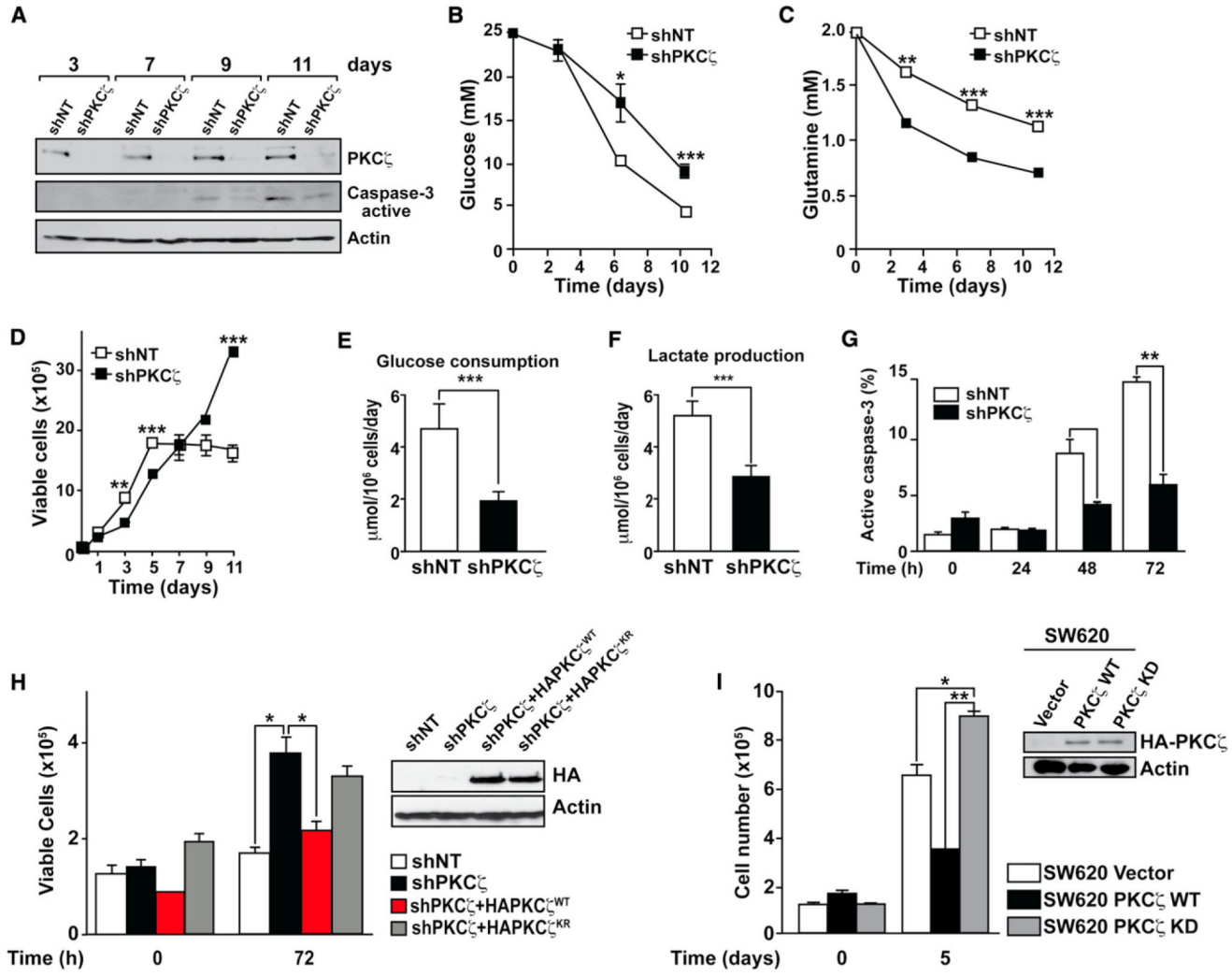

Figure 1. Control of Metabolic Stress by PKCζ

(A) Cell lysates from SW480 control (shNT) or PKCζ-deficient (shPKCζ) cells cultured under nutrient exhaustion conditions were analyzed by immunoblotting with PKCζ, active caspase-3, and actin antibodies. Results are representative of three experiments.

(B and C) Glucose and glutamine levels in the media of SW480 shNT or shPKCζ cells cultured as above. Results are the mean ± SEM (n = 3).

(D) Cell viability of SW480 shNT or shPKCζ cells cultured under nutrient exhaustion conditions. Number of cells was determined by trypan blue exclusion assay. Values are mean ± SEM of triplicates for three different experiments.

(E and F) The net consumption of glucose and production of lactate by SW480 shNT or shPKCζ cells was determined at 24 hr by enzymatic assay. Results are the mean ± SEM (n = 4).

(G) Caspase-3 activity was determined by FACS in SW480 shNT or shPKCζ cells cultured under glucose-deprived conditions. Results are the mean ± SEM (n = 3).

(H) Cell viability of SW480 shNT, shPKCζ, or shPKCζ cells reconstituted with either WT or kinase-dead PKCζ cultured under glucose-deprived conditions. Number of cells was determined by trypan blue exclusion assay. Results are mean ± SEM (n = 3). Expression of HA-tagged retroviral constructs was confirmed by immunoblotting with HA antibody (right).

(I) Cell viability of SW620 cells stably expressing WT or kinase-dead (KD) PKCζ cultured under nutrient stress conditions for 5 days. Number of cells was determined by trypan blue exclusion assay. Results are mean ± SEM (n = 3). Expression of HA-tagged retroviral constructs was confirmed by immunoblotting with HA antibody (inset).
*$p < 0.05$, **$p < 0.01$, and ***$p < 0.001$. See also Figure S1.

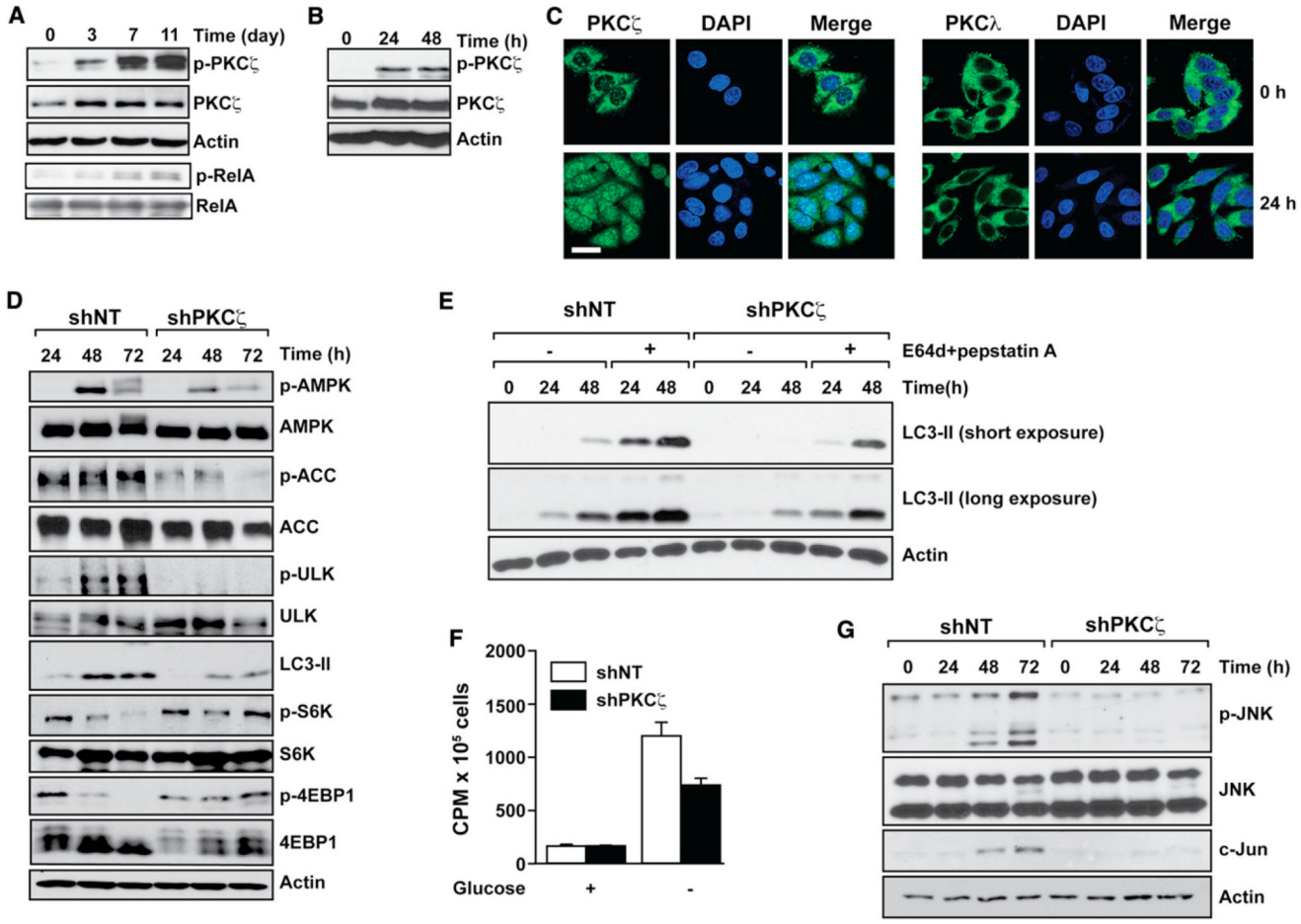

Figure 2. PKCζ Deletion Impairs Glucose Deprivation-Induced Stress Signaling

(A and B) Cell lysates from SW480 cells cultured under nutrient exhaustion (A) or under glucose-deprived (B) conditions were analyzed by immunoblotting with phospho-PKCζ-T410 (p-PKCζ), PKCζ, and actin antibodies. PKCζ activity toward RelA was determined in the corresponding immunoprecipitates (A). Results are representative of three experiments.

(C) Normal or glucose deprived for 24 hr, SW480 cells were coimmunostained for PKCζ (left) or PKCl (right) and DAPI. Scale bar, 20 μM. Images are representative of three experiments.

(D) Cell lysates from SW480 control (shNT) or PKCζ-deficient (shPKCζ) cells cultured under glucose-deprived conditions were analyzed by immunoblotting with the specified antibodies. Results are representative of three experiments.

(E) SW480 shNT or shPKCζ cells cultured under glucose-deprived conditions with or without E64d (10 μg/ml) and pepstatin A (10 μg/ml) treatment. LC3 and actin protein levels were analyzed by western blot. Results are representative of three experiments.

(F) Fatty acid oxidation was measured in SW480 shNT or shPKCζ cells cultured as above for 36 hr. Results are the mean ± SEM (n = 3). cpm, counts per minute.

(G) Cell lysates from SW480 shNT or shPKCζ cells cultured as above were analyzed by immunoblotting for phospho-JNK, c-Jun, and actin. Results are representative of three experiments.

See also Figure S2.

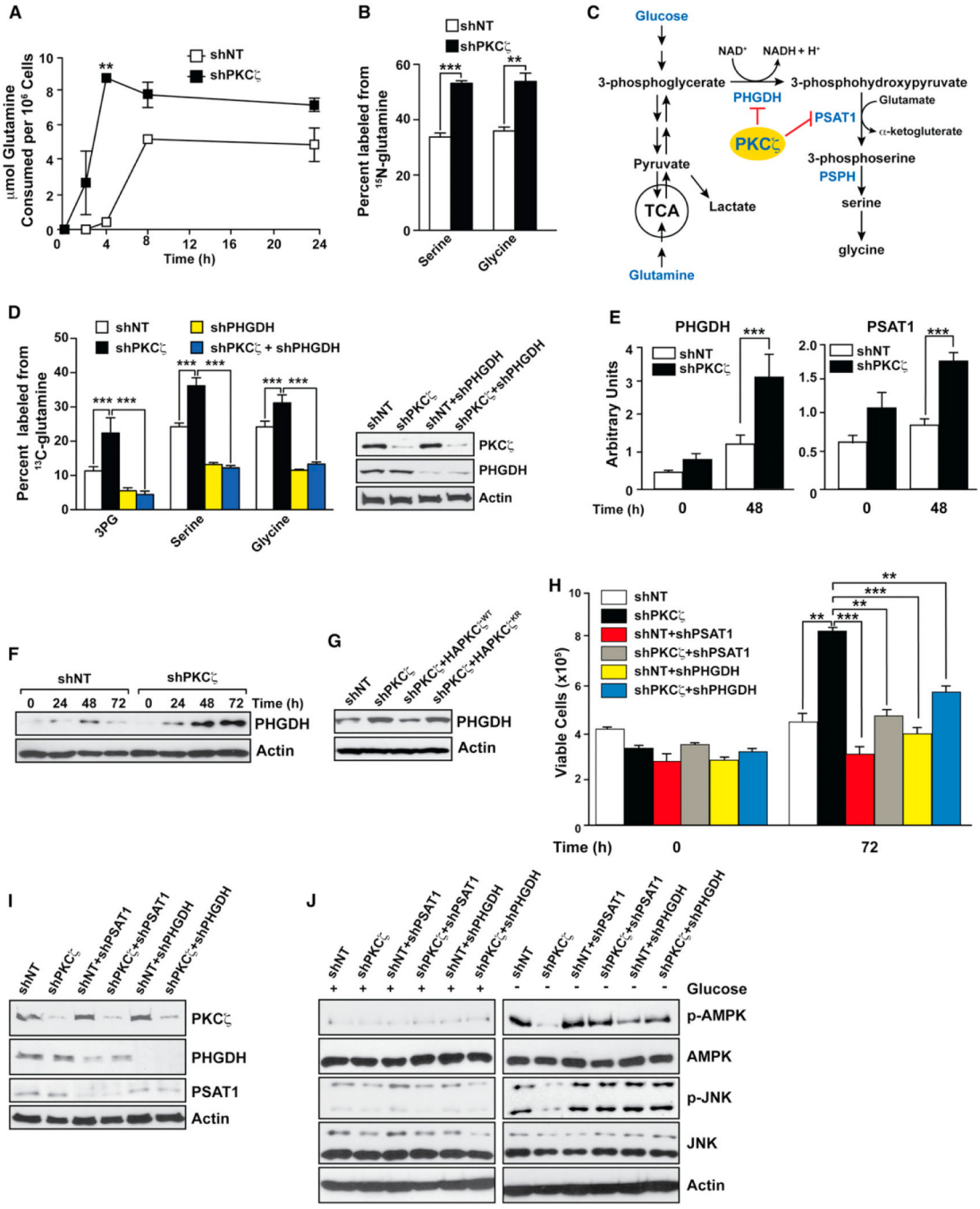

Figure 3. PKCζ Controls Metabolism by Reprogramming Glutamine Utilization

(A) The net consumption of glutamine by SW480 control (shNT) or PKCζ-deficient (shPKCζ) cells was determined by enzymatic assays over 24 hr of growth. Results are the mean ± SEM (n = 4).

(B) The percentage of glycine and serine containing ^{15}N from glutamine in shNT or shPKCζ cells after 24 hr of growth. Glutamine was isotopically labeled only at the a position. Results are the mean ± SEM (n = 2–3).

(C) Metabolic scheme depicting biosynthetic routes to serine and glycine from glucose and glutamine.

(D) The percentage of 3PG, serine, and glycine containing ^{13}C from glutamine isotopically labeled at all five carbons in SW480 shNT or shPKCζ cells after 24 hr of growth, or in these same cells in which PSAT1 or PHGDH has been knocked down. Glutamine was isotopically labeled at all five carbons. Results are the mean ± SEM (n = 4). Knockdown efficiency was determined by immunoblotting in cell lysates (right).
(E) PHGDH and PSAT1 mRNA expression was determined by quantitative PCR in SW480 shNT or shPKCζ cells cultured under glucose-deprived conditions. Results are the mean ± SEM (n = 3).
(F) PHGDH protein levels were determined by western blot in extracts of SW480 shNT or shPKCζ cells cultured under glucose-deprived conditions for indicated time. Results are representative of three experiments.
(G) PHGDH protein levels were determined by western blot in extracts of SW480 shNT, shPKCζ, or shPKCζ cells reconstituted with either WT or kinase-dead PKCζ cultured as above. Results are representative of three experiments.
(H and I) Cell viability of SW480 cells with the indicated lentiviral knockdown cultured under glucose-deprived conditions for 72 hr. Number of the cells was determined by trypan blue exclusion assay (H). Cell lysates were analyzed by immunoblotting for the specified proteins (I). Results are the mean ± SEM (n = 3).
(J) Cell lysates from SW480 cells with the indicated lentiviral knockdown were cultured under normal or glucose-deprived conditions for 72 hr after which cell lysates were analyzed by immunoblotting for the specified proteins. Results are representative of three experiments.
*$p < 0.05$, **$p < 0.01$, and ***$p < 0.001$. See also Figure S3 and Table S1.

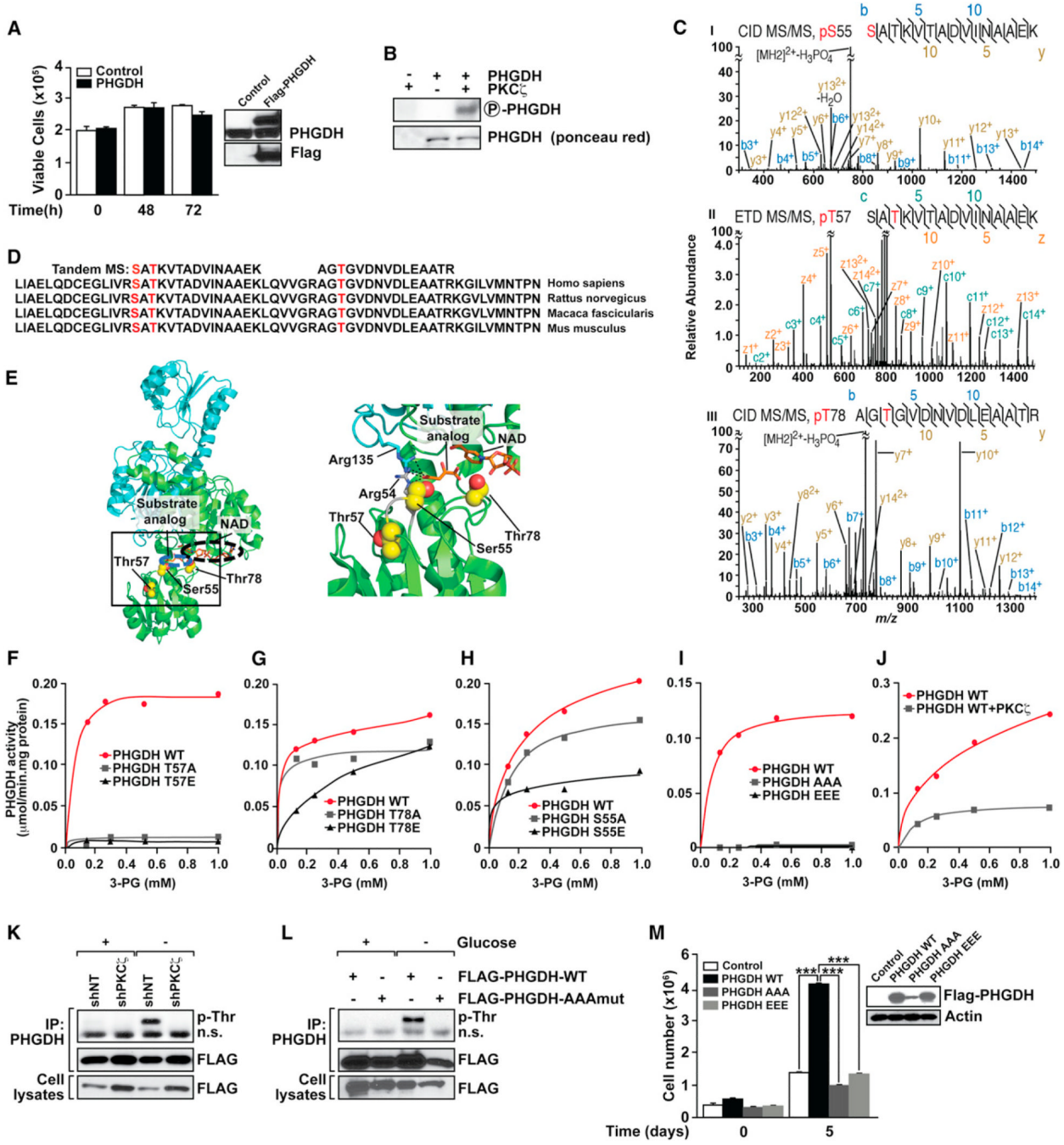

Figure 4. PKCζ Phosphorylation Regulates PHGDH Activity

(A) Cell viability of SW480 cells stably expressing PHGDH cultured under glucose-deprived conditions. Results are the mean ± SEM (n = 3). Expression of Flag-tagged PHGDH was confirmed by immunoblotting with Flag antibody (inset).

(B) PKCζ phosphorylates PHGDH in vitro.

(C) MS/MS spectra of phosphopeptides containing the phosphoserine (pS) 55 (I), phosphothreonine (pT) 57 (II), or the pT78 (III) site of PHDGH. Fragment ions are shown, as is the sequence coverage due to identified fragment ions. All of the highest peaks were explained, but for clarity, they are not all annotated. m/z, mass-to-charge ratio.

(D) Ser55, Thr57, and Thr78 phosphorylation sites are highly conserved among human, rat, monkey, and mouse. Identified phosphopeptides are shown above the sequence alignments.
(E) Ser55, Thr57, and Thr78 in the crystal structure of human PHGDH. Overall view of the PHGDH dimer (Protein Data Bank ID code 2g76) with the two chains of the dimer colored in green and cyan, respectively. The relative positions of NAD (black circle) and substrate analog D-malate (blue circle), as well as Ser55, Thr57, and Thr78 (red and yellow spheres) are indicated (left). Close-up view of the substrate binding site (right). The loop affected by mutation of Thr57 is colored gray, and Arg54 and Arg135, which participate in binding of the substrate analog, are indicated in stick representation (right).
(F–I) PHGDH enzymatic activities of T→A and T→E mutations of Thr57 (F) and Thr78 (G) sites, and S→A and S→E mutations of Ser55 site (H), and Ser55/Thr57/Thr78 sites → AAA and Ser55/Thr57/Thr78 sites→ EEE mutations (I). Results are representative of three experiments.
(J) PHGDH activity after in vitro phosphorylation by recombinant PKCζ.
(K) Lysates and immunoprecipitates (IP) from SW480 shNT and shPKCζ cells cultured under normal or glucose-deprived conditions for 48 hr were analyzed by immunoblotting to determine the level of phosphorylated Thr. Results are representative of three experiments. n.s., nonspecific.
(L) Lysates and immunoprecipitates from SW480 cells stably expressing Flag-PHGDH or Flag-PHGDH AAA mutant cultured under normal or glucose-deprived conditions for 48 hr were analyzed by immunoblotting to determine the level of phosphorylated Thr. Results are representative of three experiments.
(M) Cell viability of MDA-MB-231 cells stably expressing PHGDH WT, PHGDH AAA mutant, or EEE mutant cultured under serine-deprived conditions for 5 days. Number of cells was determined by trypan blue exclusion assay. Results are mean ± SEM (n = 3). ***$p < 0.001$.
See also Figure S4.

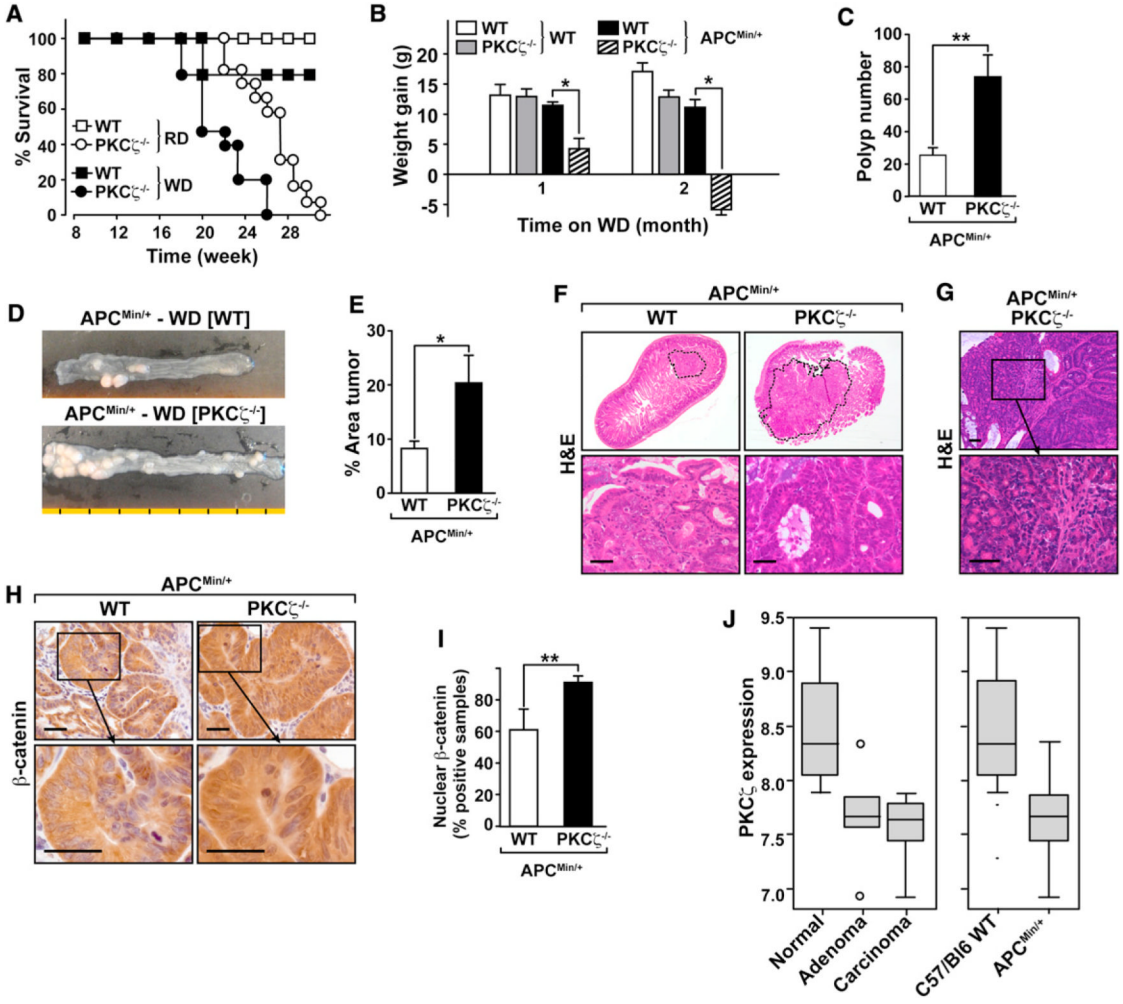

Figure 5. PKCζ Deletion Enhances Intestinal Tumorigenesis in APC$^{Min/+}$ Mice

(A) Kaplan-Meier survival graph for PKCζ$^{+/+}$/APC$^{Min/+}$ (squares) and PKCζ$^{-/-}$/APC$^{Min/+}$ (circles) fed with a regular diet (RD; open symbols) or the WD (closed symbols).

(B) Graph showing changes in total body weight after animals were fed with the WD for the indicated times. White bars represent PKCζ$^{+/+}$, gray bars indicate PKCζ$^{-/-}$, black bars show PKCζ$^{+/+}$/APC$^{Min/+}$, and striped bars demonstrate PKCζ$^{-/-}$/APC$^{Min/+}$. Values represent mean ± SEM of 14 mice per group.

(C) Number of polyps in distal small intestine sections of PKCζ$^{+/+}$/APC$^{Min/+}$ (WT) and PKCζ$^{-/-}$/APC$^{Min/+}$ mice fed with the WD for 2 months. Values represent mean ± SEM of at least 14 mice per group.

(D) Representative intestines from APC$^{Min/+}$ mice with different genotypes. Each segment is equivalent to 1 cm.

(E) Graph showing the area of polyps in distal small intestine sections of PKCζ$^{+/+}$/APC$^{Min/+}$ (WT) and PKCζ$^{-/-}$/APC$^{Min/+}$ mice fed with the WD for 2 months. Values are mean ± SEM of at least 14 mice per group.

(F) Upper: a lower magnification of H&E of distal small intestine sections of PKCζ$^{+/+}$/APC$^{Min/+}$ (WT) and PKCζ$^{-/-}$/APC$^{Min/+}$ mice. Tumors are delineated by a dashed line. Lower: a higher magnification of low-grade adenoma (left) and high-grade adenoma (right). Scale bars, 50 μm.

(G) H&E of distal small intestine section of PKCζ$^{-/-}$/APC$^{Min/+}$ mice showing intramucosal adenocarcinoma. Lower: shows a higher magnification. Scale bars, 50 μm.
(H) Immunodetection of β-catenin in tumors located in distal small intestine of PKCζ$^{+/+}$/APC$^{Min/+}$ (WT) and PKCζ$^{-/-}$/APC$^{Min/+}$ mice. β-Catenin staining was stronger in cytoplasm and nuclei of PKCζ$^{-/-}$ mice. Scale bars, 50 μm.
(I) Graph showing the number of samples staining positive for nuclear β-catenin in tumors located in distal small intestine sections of PKCζ$^{+/+}$/APC$^{Min/+}$ (WT) and PKCζ$^{-/-}$/APC$^{Min/+}$. Values represent mean ± SEM of at least ten mice per group.
(J) PKCζ mRNA expression levels are significantly decreased in adenomas and carcinomas from APC$^{Min/+}$ mice, as compared to normal tissue. t test, $p = 0.01$ (WT, n = 6; APC$^{Min/+}$, n = 10).
*$p < 0.05$ and **$p < 0.01$.

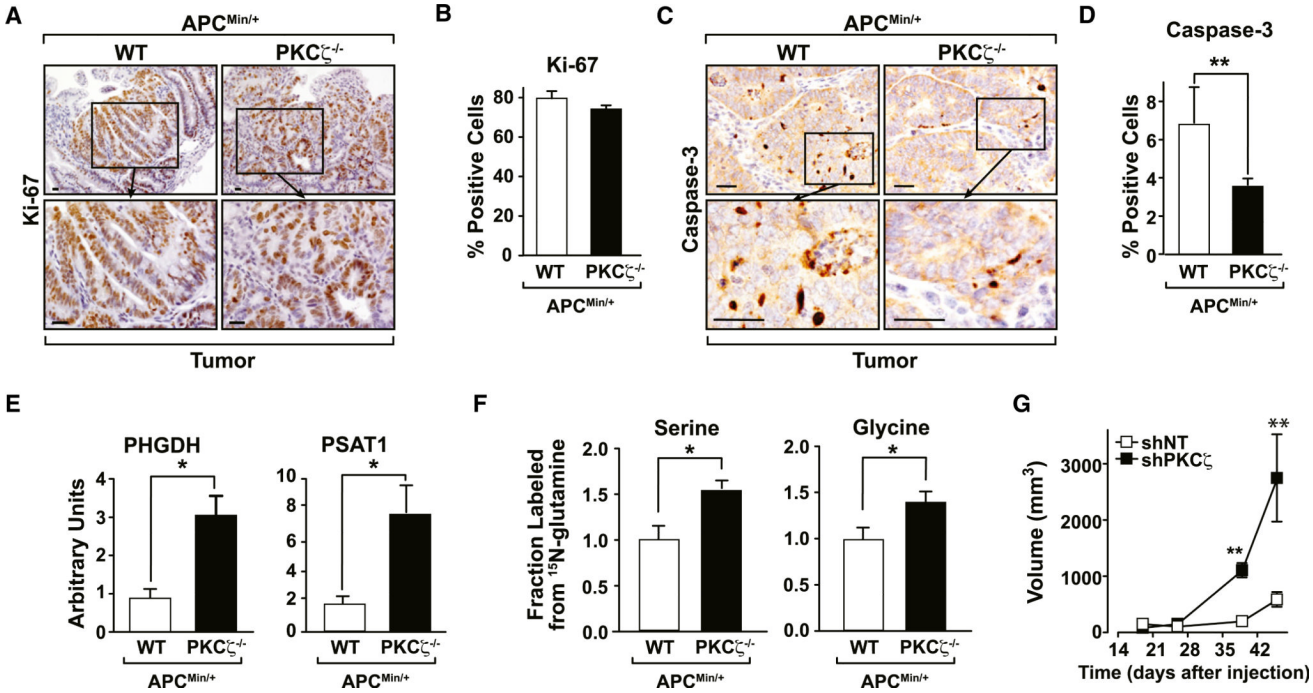

Figure 6. PKCζ Deletion Reduces Apoptosis in APC$^{Min/+}$ Tumors

(A) Immunostaining for Ki67 in tumors located in distal small intestine sections of PKCζ$^{+/+}$/APC$^{Min/+}$ (WT) and PKCζ$^{-/-}$/APC$^{Min/+}$ (KO) mice. Scale bar, 50 μm.

(B) Number of cells staining positive for Ki67 in tumor tissue. Values represent mean ± SEM of at least ten samples per group.

(C) Immunostaining for caspase-3 in tumors located in distal small intestine sections of PKCζ$^{+/+}$/APC$^{Min/+}$ and PKCζ$^{-/-}$/APC$^{Min/+}$ mice. Scale bars, 50 μm.

(D) Number of cells staining positive for caspase-3 in tumor tissue. Values represent mean ± SEM of at least 14 samples per group.

(E) Quantitative PCR assays of PSAT1 and PHGDH were measured in distal small intestine sections of PKCζ$^{+/+}$/APC$^{Min/+}$ (WT) and PKCζ$^{-/-}$/APC$^{Min/+}$ mice. Results are the mean ± SEM (n = 3).

(F) The fraction of glycine and serine containing ^{15}N from glutamine following 24 hr of incubation in tumor explants from PKCζ$^{+/+}$/APC$^{Min/+}$ (WT) and PKCζ$^{-/-}$/APC$^{Min/+}$ mice. Glutamine was isotopically labeled only at the a position. Results are the mean ± SEM (n = 5–6).

(G) SW480 shNT or shPKCζ cell suspensions (5 × 10^6) were intradermally injected into each flank of nude mice. Tumors were allowed to develop for 46 days. Tumor size was determined by direct measurement with a caliper and calculated by the formula: (widest diameter × smallest diameter^2)/2. Results are mean ± SEM (n = 5).

*p < 0.05 and **p < 0.01.

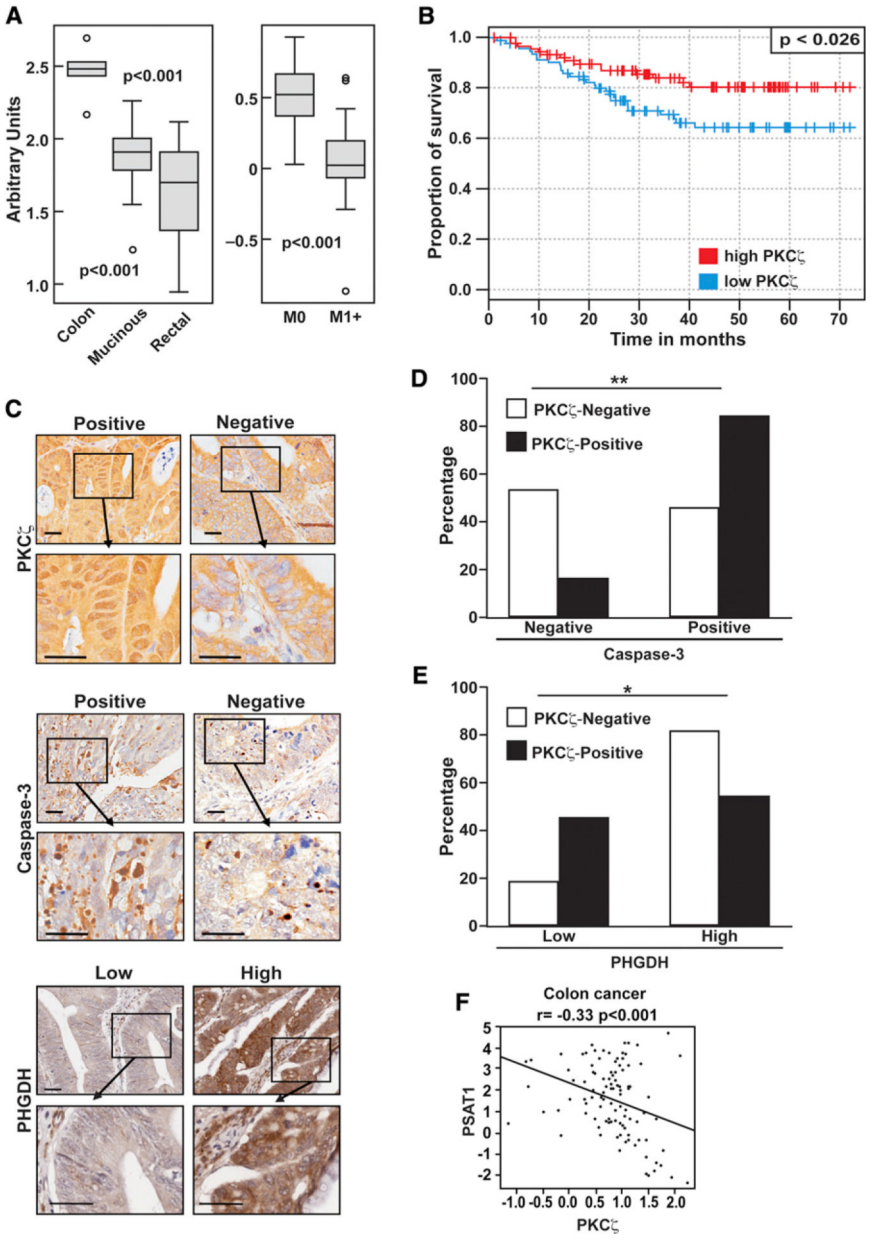

Figure 7. Tumor Suppressor Role of PKCζ in Human Colon Cancer

(A) Gene expression analysis of PKCζ in human colon cancer samples in public microarray data.

(B) Kaplan-Meier curves comparing the survival of patients with high versus low expression of PKCζ.

(C) Representative sections of PKCζ, caspase-3, and PHGDH immunostaining. Scale bars, 50 μm.

(D) Associated correlation of caspase-3 and PKCζ expression in human colon cancer TMA. Nuclear PKCζ expression positively correlates with active caspase-3 levels. **p < 0.01.

(E) Associated correlation of PHGDH and PKCζ expression in human colon cancer TMA. Nuclear PKCζ expression negatively correlates with PHGDH levels. *p < 0.05.

(F) Negative correlation between PKCζ and PSAT1 mRNA levels in human colorectal carcinomas.